Cement and Concrete Composites 136 (2023) 104900

Contents lists available at ScienceDirect

Cement and Concrete Composites

journal homepage: www.elsevier.com/locate/cemconcomp

Performance and interaction of sodium silicate activated slag with lignosulfonate superplasticiser added at different mixing stages

Jun Ren [a,b], Qi-Zhi Zhou [b], Chang-Hui Yang [c], Yun Bai [b,*]

[a] School of Architecture and Planning, Yunnan University, Kunming, 650500, PR China
[b] The Advanced & Innovative Materials (AIM) Group, Department of Civil, Environmental and Geomatic Engineering, University College London, London, WC1E 6BT, UK
[c] College of Materials and Engineering, Chongqing University, 400045, PR China

ARTICLE INFO

Keywords:
Alkali activated cement
Superplasticiser
Rheology
Granulated blast-furnace slag
Adsorption

ABSTRACT

This paper investigated the effect of adding lignosulfonate (LS) superplasticiser at the different stages of mixing on the workability and rheological behaviour of sodium silicate activated slag (SSAS) in order to find a practically feasible approach to tackling the incompatibility issue between superplasticiser and alkaline activator. In addition to rheology and minislump tests, adsorption, zeta potential and environmental scanning electron microscopy tests were also undertaken to understand the interactions between the lignosulfonate and the fresh SSAS in order to reveal the mechanisms behind the observation. The results show that adding the LS and the activator separately at the different stages of mixing can significantly improve both the initial minislump and 60-min minislump retention due to the increased adsorption of LS and the improved dispersion of slag particles, with the prior addition of LS better than the delayed addition. However, a nonlinear rheological behaviour of SSAS was observed in the LS-superplasticised SSAS under separate addition and, consequently, modified Bingham model was found to be more suitable for describing this kind of rheological behaviour.

1. Introduction

Rheological behaviour and fresh properties of concrete are not only important for transporting, placing, compacting and finishing of fresh concrete, but also essential for hardened concrete to achieve desirable mechanical and durability properties. Due to these importance, the rheological behaviour of Portland cement (PC) - based cementitious materials has been widely studied in the past and most of the results show that fresh PC concrete is a thixotropic material which is featured by a decrease in viscosity when a certain amount of shear is applied and a gradual recovery of viscosity when the shear is removed [1]. To achieve a good understanding of the fresh properties of concrete, considerable efforts have been made to model the rheological behaviour of PC concrete [2]. It is now generally agreed that, at a moderate/high shear rate, the rheological behaviour of PC-based cementitious materials without chemical admixture, can be best fitted by the Bingham model (Equation (1)) [3], which depicts a linear relationship between shear stress and shear rate. In addition, the yield stress, which is defined as the intercept in the Bingham model in Equation (1), can be considered as the transition point below which the substance behaves as a solid and above which it becomes a fluid [4,5], resulting from the attractive inter-particle forces responsible for the flocculation and/or from hydration [6,7]. Thus, substances with a lower yield stress reflect a better dispersion and fluidity. On the other hand, the plastic viscosity, defined as the slope in the Bingham model, depends largely on the volume friction of solid particles and the packed density [8]. As a result, a low plastic viscosity might cause segregation [9]. However, at a low shear rate, especially in the presence of superplasticiser (SP), the rheological behaviour may deviate away from the linear relationship as defined by the Bingham model. This is, in particular, the case when SP is added together with other chemicals. For example, when higher dosages of SP and viscosity modifying agent are added in self-compacting concretes, negative yield stress and non-linear shear thickening (in which case the plastic viscosity increases/decreases with the increase of shear rate) have been reported [10,11]. However, it must be emphasized that the negative yield stress does not have any physical meaning. It is, thus, questionable whether the linear Bingham model is still suitable to fit these nonlinear rheological behaviours. To tackle these issues, nonlinear rheological models, such as the modified Bingham model (MB model, Equation (2)) or the Herschel-Bulkley model (HB model, Equation (3))

* Corresponding author.
E-mail address: yun.bai@ucl.ac.uk (Y. Bai).

https://doi.org/10.1016/j.cemconcomp.2022.104900
Received 21 May 2022; Received in revised form 28 November 2022; Accepted 12 December 2022
Available online 13 December 2022
0958-9465/© 2022 The Authors. Published by Elsevier Ltd. This is an open access article under the CC BY license (http://creativecommons.org/licenses/by/4.0/).

(as shown below), have been considered as the most favourable alternative [9,11,12]. In these two models, the value of exponent n (MB model) and the term c/μ (HB model) can be applied to indicate the non-linear rheological behaviour of the materials, e.g., shear thinning ($n < 1$ or $c/\mu < 0$), shear thickening ($n > 1$ or $c/\mu > 0$) and Bingham behaviour ($n = 1$or $c/\mu = 0$) [13,14].

$$\tau = \tau_0 + \mu \bullet \dot{\gamma} \quad (1)$$

$$\tau = \tau_0 + \mu \bullet \dot{\gamma} + c \bullet \dot{\gamma}^2 \quad (2)$$

$$\tau = \tau_0 + K \bullet \dot{\gamma}^n \quad (3)$$

Where: τ stands for shear stress (Pa); τ_0 for yield stress (Pa); μ for plastic viscosity (Pa·s); $\dot{\gamma}$ for shear rate (s^{-1}); c for second order parameter (Pa s^2); K for consistency factor (Pa·s ^{n}); and n for exponent (−).

Alkali-activated slag (AAS), which typically consists of ground granulated-blast furnace slag (GGBS for short hereafter) and alkaline activators, has received increased attention worldwide due to its sustainable nature and superior performance in some aspects over PC, such as low heat of hydration, high early strength and excellent durability in some aggressive environments [15–19]. In recent years, attempts have also been made by the authors to explore its cast-in-situ application for reinforced structures [20] as well as the immobilisation of nuclear wastes [21]. Slag, a by-product from iron manufacture, is often in the form of granulated glassy calcium-magnesium aluminosilicate powder. It can react with alkaline activators, such as sodium silicate and sodium hydroxide, to form a cementitious binder at ambient temperature. However, compared to PC system, AAS involves a different cement chemistry and reaction mechanism. For instance, a gel-like matrix is formed through a fast 'through solution' precipitation in sodium silicate activated slag, whilst needle-like products are formed through a slow dissolution-precipitation mechanism of a 'torpotactic' growth of C–S–H in PC systems [22]. Additionally, the composition of the pore solution and surface chemistry of AAS also differ from those of PC systems [23,24]. All these could lead to different inter-particle forces which could partly explain the more viscous nature and higher resistance to shear characteristics of AAS as compared to PC-based systems [15]. Consequently, the rheological behaviour of fresh AAS might be affected and the suitability of the Bingham model for describing the rheological behaviour of AAS becomes questionable [25,26]. On the other hand, to develop high performance AAS concretes, attempts have also been made by researchers to add SPs into AAS systems [27,28]. However, the current commercially available SPs have been developed based on the chemistry of PC-based cementitious materials and it may not be suitable for AAS systems due to the different cement chemistry involved [29]. For example, it was found that adding polycarboxylate-based SP was less efficient in reducing the yield stress of sodium silicate-activated slag (SSAS) compared to its performance in PC systems [25]. Whilst the lignosulfonate-based (LS) SP has demonstrated some limited improvement in the workability of AAS, the workability retention is considered to be insufficient [30]. The reduced performance of SPs designed for Portland Cement in AAS systems has been mainly attributed to two reasons. The first is the competitive adsorption between the negatively charged alkaline activator and the SPs (which is also negatively charged); the second is the instability and, hence, the change of the chemical structure SPs designed for Portland Cement in highly alkaline environment [25,27,31]. It should be highlighted that the latter effect could become even worse if the SP is directly added into the alkaline activator before mixing with slag due to the strong alkaline nature of the activator [27].

In an attempt to address the above issues, some preliminary studies were carried out by the authors to add SP at different stages of mixing in order to avoid the competitive adsorption between SP and activator as well as to improve the stability of SP in alkaline activator [32]. This approach is very much similar to that adopted in PC systems to improve the workability of concrete by delayed addition of SP during the mixing which allows the time for gypsum and clinker to react without competing with SP. However, it has been shown that by delayed adding SP, the rheological behaviour of the PC-based cementitious system was changed [33]. Hence, it is likely that adding SP and alkaline activator at different time intervals during the mixing stage could also make the rheological behaviour of AAS more complex and uncertain.

The aim of this study is, therefore, to investigate the rheological behaviour and some fresh properties of SSAS when a lignosulfonate SP was added at the different stages of mixing. The rheological behaviour of the fresh SSAS was then analysed using the flow curves obtained from the rheology tests by fitting into different rheology models. Moreover, the interaction between the lignosulfonate SP and the fresh SSAS was also characterised by adsorption, zeta potential and environmental scanning electron microscopy (ESEM) tests. Based on the information obtained, the possible mechanisms involved are then proposed and discussed in this paper.

2. Experimental

2.1. Materials

The slag complies with BS EN 15167–1:2006 and supplied by Civil and Marine Ltd. UK (now Hanson Heidelberg Cement Group) was used in this study. Its chemical composition obtained by X-ray fluorescence spectroscopy is reported in Table 1. It is a granulated product with a specific surface area of 527 m^2/kg (based on Blaine method) and can be categorized as a neutral slag according to its basicity coefficient, K_b= (CaO + MgO)/(SiO_2 + Al_2O_3), which equals to 0.96. Moreover, its particles size distribution was obtained by a Mastersizer (Mastersizer 2000, Malvern, UK) and is presented in Fig. 1. As shown in the figure, 65.62% of the slag was smaller than 10 μm.

A liquid sodium silicate solution with a silica modulus of 2.58 was obtained from Charles Tennant & Co Ltd and its chemical and physical properties are shown in Table 2. The sodium silicate solution was then modulated to a modulus (molar ratio of SiO_2 to Na_2O) of 1.5 by adding sodium hydroxide (NaOH, obtained from Tennants Distribution), which was then used as an alkaline activator in this study. A lignosulfonate derivation superplasticiser (LS), a dark brown dry powder supplied by Tianjin Jiangong Special Material Co. Ltd., was used as a superplasticiser.

2.2. Sample preparation

All the samples were prepared and mixed in 5L planar-action high-shear mixer, and a lower speed (140 rpm) was employed during the whole mixing procedure. The water to slag ratio of all the mixes was fixed at 0.45 which was obtained from trial mixes to ensure sufficient workability could be achieved for the rheology tests. The dosages of LS were controlled at 0, 0.4, 0.8, 1.2, 1.6, and 2.0% (by the mass of slag). The liquid sodium silicate with a silica modulus of 1.5 was used as the activator and its content was fixed at 4 wt % (counted as Na_2O equivalent) by the mass of slag. Both the activator and the LS were firstly dissolved in water. When the activator and the LS were added separately at the different stages of mixing, i.e., separate addition as described below, the total mixing water was split into 2/3 and 1/3 for the first and second components (as indicated in Fig. 1) respectively, and the activator or the LS were then dissolved in water and added into the mixer accordingly during the mixing stage. Three different approaches of adding LS were investigated in this study, and they are named accordingly as: 1) ***simultaneous addition (SA)***: adding LS and activator together when mixing with slag; 2) ***delayed addition (DA)***: adding activator to slag first and then LS at a 3 min interval; and 3) ***prior addition (PA)***: adding LS to slag first, then activator at a 3 min interval. The 3-min interval was determined based on the results obtained from the preliminary experiments. The mixing procedure of all the mixes was

Table 1
Chemical composition of slag.

%	CaO	SiO_2	Al_2O_3	MgO	Sulphide	TiO_2	Mn_2O_3	Na_2O	Fe_2O_3	K_2O	LOI
Slag	39.40	34.30	15.00	8.00	0.80	0.70	0.50	0.45	0.40	0.38	0.70

LOI.: loss on ignition.

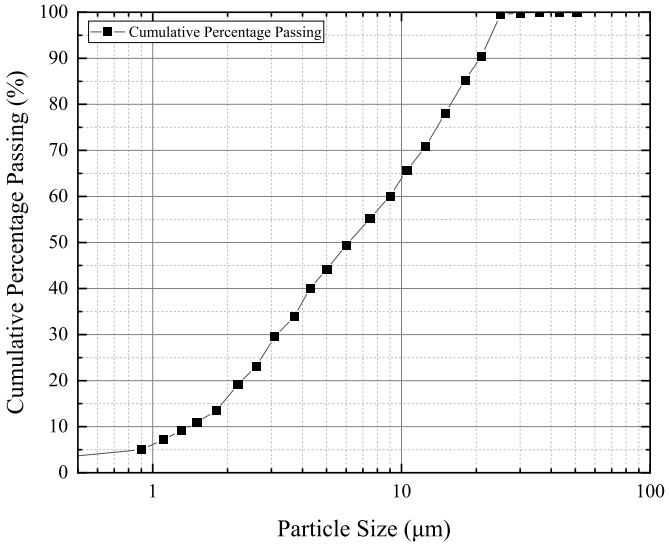

Fig. 1. Particle size distribution of slag.

strictly controlled throughout this study in order to compare the rheological behaviour on a like-for-like basis and the details of this are schematically presented in Fig. 2. The total mixing time for the three addition methods was all fixed for 5 min.

2.3. Test procedure

2.3.1. Minislump test

The minislump test was carried out with a PVC plate and a cone with a lower inner diameter of 38.1 mm, an upper inner diameter of 19 mm and a height of 57.2 mm by following Palacios's method [28]. The diameters of the spread from the minislump test were measured at two perpendicular directions and the average diameter was reported. All the minislump measurements were first conducted at 7 min after mixing, which is referred to as the '***initial minislump***' in this paper. In addition, to assess the workability retention capacity of the SSAS, the minislumps were also measured over time at 15, 30 and 60 min since mixing.

2.3.2. Rheological test

The rheological behaviour of the SSAS pastes was determined with a rheometer, Viscotester 550, under all the three SP addition methods (namely, *SA, DA* and *PA*). Immediately after mixing (i.e., at the 5th minute shown in Fig. 1), approximate 800 ml freshly mixed paste was transferred into a 1000 ml plastic cup (95 mm in diameter and 180 mm in length) and then fixed into the sample holder of the rheometer before inserting a six-bladed vane (40 mm in diameter and 60 mm in length) to establish the relationship between the shear stress and the shear rate. The samples were then subjected to a cycled measuring procedure as proposed by Palacios et al. [25] as follows. The shear rate was kept constant at 150 s^{-1} for 2 min during the pre-shearing, then up-ramped from 0 to 10 s^{-1} in 1 min, continually raised from 10 to 150 s^{-1} in 1 min and finally reduced from 150 to 0 s^{-1} in 1 min. The results were recorded by an in-house developed software. To ensure that reliable data can be obtained from the rheological tests, the 'pure' AAS was tested for five times to check the repeatability of the measurement first [34]. Once the reliability requirements were met, the flow curves of the SSAS pastes under different SP addition methods were then obtained. The area of the hysteresis loop of the flow curve was then calculated which was used to quantitatively analyse the structural breakdown of the paste [35]. Moreover, the down curve of the flow curves, which is believed to be able to reflect the rheological properties of cementitious materials [36], were used to fit different rheological models as described by Equations (1)–(3).

2.3.3. Adsorption test

The amount of LS adsorbed by SSAS was determined by a UV-spectrophotometer (Camspec 550) at a wavelength of 286 nm. Prior to the experiments, a calibration curve was established by plotting the concentrations of added LS against the absorption of UV light by the

Table 2
Chemical and physical properties of sodium silicate 'Crystal 0503'.

Twaddell	Beaume	Specific gravity	SiO_2:Na_2O weight ratio	SiO_2:Na_2O mole ratio	Na_2O%	SiO_2%	Total solid%	Viscosity (20 °C)
100.00	48.30	1.50	2.50	2.58	12.45	31.10	0.45	400.00 P

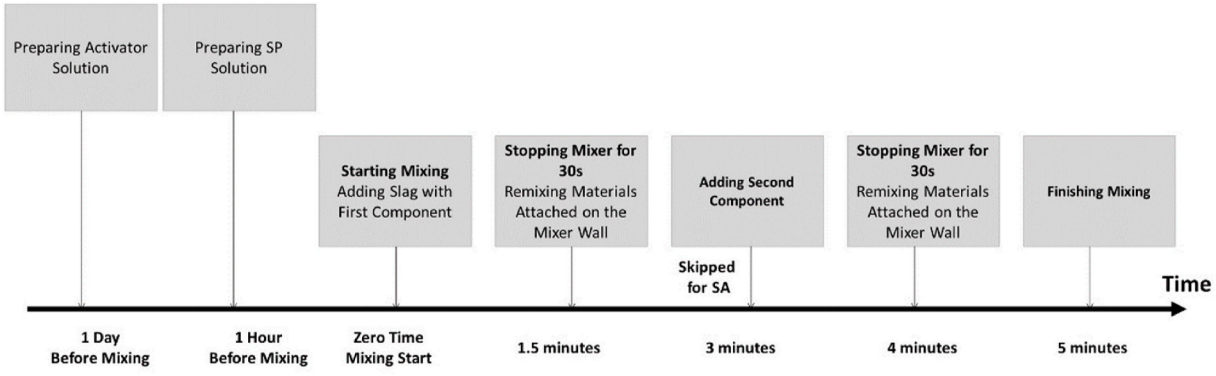

Fig. 2. Flow chart of mixing procedure.

corresponding LS solutions. To overcome the matrix effect, the solution was prepared by dissolving the LS, ranging from 0.025 mg/ml to 0.150 mg/ml, in the supernatant of SSAS paste. To measure the amount of LS adsorbed by SSAS, mixes consisting of 5 g of slag, 1.04 g sodium silicate solution (4 wt% Na_2O equivalent by the mass of slag), 19.45 g of water and different dosages of LS, namely 0, 0.4, 0.8, 1.2, 1.6, and 2.0% by the mass of slag, were prepared by hand mixing. The suspension of each mix was then centrifuged at 700 rpm for 3 min before being filtered by a quantitative filter paper. The obtained solution was then diluted with deionised water to the measurable range of UV-spectrophotometer. The amount of LS adsorbed by SSAS was finally calculated from the difference of the LS concentrations before and after mixing with SSAS.

2.3.4. Zeta potential test

The change in the electrostatic properties of the SSAS was investigated through the measurement of zeta potential. The suspensions used for the zeta potential test were prepared by dispersing 1 g of slag and the corresponding amount of activator (as detailed in Section 2.2) in 200 ml deionised water at different dosages of LS by hand mixing for 5 min. The zeta potential of the SSAS suspension was then determined at 20 °C using a Malvern Nano ZS90 (Malvern Instruments Ltd., UK).

2.3.5. ESEM

The dispersion of the freshly mixed paste samples was observed by Environmental scanning electron microscopy (ESEM) in a FEI Quanta 200 Scanning Electron Microscope at 20 kV. Mixes containing approximately 0.5 g of slags and corresponding SP solution and activator were firstly mixed in a beaker outside the environmental chamber of the ESEM by hand for 3 min. After that, the fresh paste was rapidly poured into a steel sample holder before being placed into the sample chamber in the ESEM. The observation was then started at 10 min after mixing under the ESEM mode with the stage being cooled to 5 °C and the water vapour used as imaging gas at 5.0 torr pressure. To quantitatively analyse the dispersion of the slag particles, the Heywood diameter of slag particles, which is referred to the diameter of a circle with equal area of the shape of slag particles, were generated from the ESEM images using the software 'Image J' [37,38]. For each mix, ten ESEM images were quantitatively analysed. It should be pointed out that, in this method, the outline of the particle shape was automatically identified and transferred to the particle size and area. Therefore, it has been confirmed to be an effective approach for identifying the agglomeration behaviour of particles [39].

3. Results and discussion

3.1. Workability

The results of the initial minislump tests of SSAS with the LS added at the different stages of mixing are shown in Fig. 3. It is obvious that compared with the reference (i.e., the mix containing 0% of LS), regardless of the LS addition methods, adding LS increased the initial minislump spread and this was increased with increasing dosage of LS. However, only less than 10 mm increment was observed in the initial minislump from the simultaneous addition with even up to 2.0% of LS, which was less significant than those obtained from the separate addition methods (i.e., both delayed and prior additions). In contrast, the spread diameters of the initial minislump obtained from both prior and delayed addition methods were at least 10 mm higher than that of the *SA*, which correlates well with the yield stress results (as presented in Figs. 7(a), 8(a) and 9(a) below).

In addition to the initial minislump measurements, the change of the minislump was also monitored over time at 15, 30 and 60 min to assess the workability retention of SSAS when the LS was added at the different mixing stages. The minislump results of SSAS mixes over 60 min when 1.2% of LS, which was close to its saturation dosage, was added by different addition methods are shown in Fig. 4. It should be noted that similar trends were also observed at other LS dosages (results not shown in this paper). To clearly identify the effect of LS on the workability retention of SSAS, the minislump of the SSAS without LS was also monitored over the same period of time and the results are presented together in Fig. 4. It is evident that, without adding LS, the minislump of SSAS was the lowest throughout the 60 min period. Moreover, it also showed the poorest workability retention. When the LS was added by *SA*, although both the initial minislump and minislump retention of SSAS were slightly improved compared with the SSAS without LS over 60 min, they were still poorer compared with the separate addition methods. As can be seen from Fig. 4, although the initial minislump of the SSAS with *SA* reached a high value of 120 mm, this was dropped to

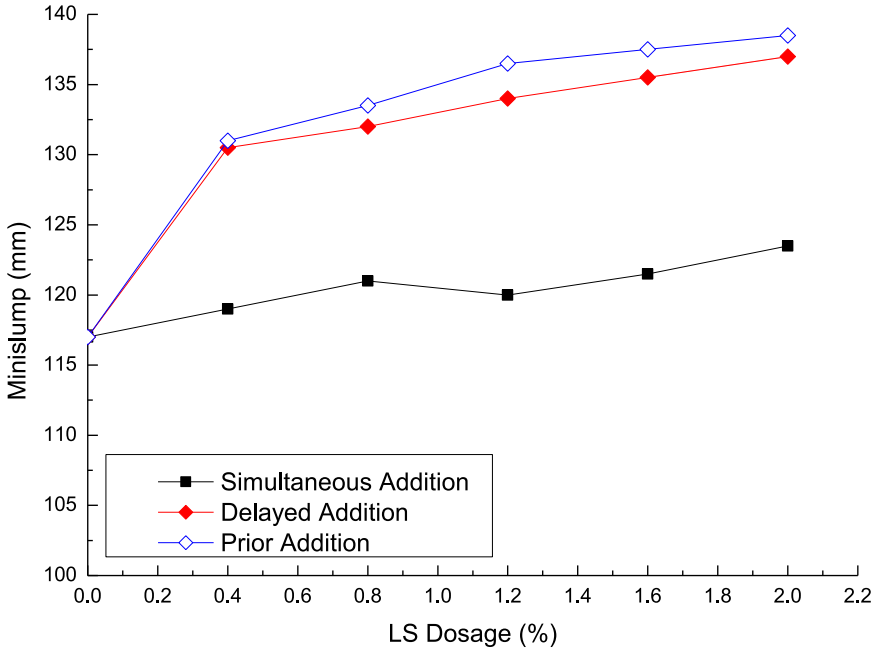

Fig. 3. Initial minislump of SSAS with different addition methods.

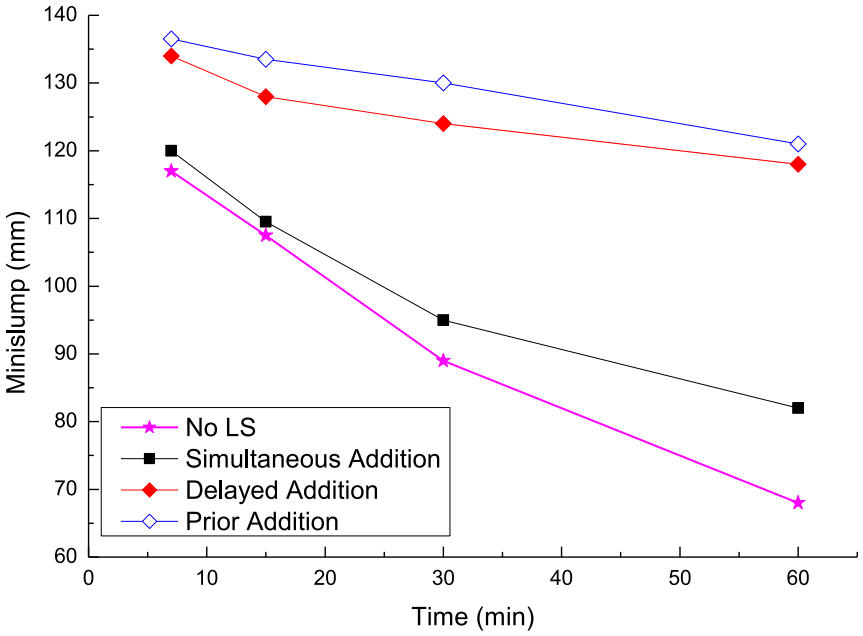

Fig. 4. Minislump of SSAS with different addition methods over time (1.2% LS dosage by the mass of slag).

less than 85 mm at the 60th minute, representing an approximate 30% minislump loss, which is much worse, both in terms of the initial minislump and workability retention, than the SSAS with separate addition methods. Similar result was also reported by Palacios and Puertas when melamine-based superplasticiser and sodium silicate activator were added by an *SA* method [28]. On the contrary, when the activator and the LS were added separately (i.e., by *DA* or *PA*), the workability retention was much improved, with only less than 12% minislump loss being observed. Moreover, slightly better workability retention was obtained from *PA*.

The above results indicate that the separate addition methods can not only enhance the initial workability, but also can improve the workability retention of LS-superplasticised SSAS. This is, in particular, the case when the LS SP is added before the alkaline activator during the mixing.

3.2. Rheological behaviour

3.2.1. Flow curve and thixotropic behaviour

The flow curves of the SSAS pastes obtained from different LS addition methods at a LS dosage of 1.2% are shown in Fig. 5. The flow curve of the SSAS without adding SP (i.e., no LS. Hereinafter referred to as 'pure' SSAS) was also presented in Fig. 5 (a) for comparison purpose. Additionally, by integrating the area between the up-curve and down-curve of the paste, the thixotropic area of the SSAS was calculated by following the method proposed by Chen and co-workers [40] as shown in Fig. 5 (b). It can be seen that without LS, the hysteresis loop of the 'pure' SSAS was larger than those of the LS-superplasticised SSAS pastes. As the area of the thixotropic loop is related to the energy needed to break down the reversible flocculation of particles [41], the reduced area of the loop when LS SP is added suggests that it becomes easier for the particles to be deflocculated. It should be noted that with increasing LS dosage, the thixotropic area was increased under *SA*, while that of the *DA* or *PA* was not obvious. This phenomenon could be due to the complex interactions among the LS, activator and slag, which should be further explored. Furthermore, among the three LS-superplasticised SSASs, the paste with *SA* showed a much larger area of thixotropic loop than those of *DA* and *PA*, indicating a better dispersion of the slag particles was achieved by both *DA* and *PA*. However, it should be noticed that the area of the thixotropic loop of *SA* was only slightly smaller than that of 'pure' SSAS, indicating that SA is not efficient in dispersing slag particles in SSAS compared to the separate addition methods. From the results shown in Fig. 5 (a), it is also evident that not only the addition of LS, but also its adding method, can change the down-curve of the paste. For example, the down-curve of both the 'pure' paste mixed without SP and the paste mixed by *SA* showed a near-linear relationship between the shear stress and the shear rate, while those mixed by *PA* and *DA* showed a non-linear relationship (further details can be seen in Fig. 6). Similar patterns were also identified at the other LS dosage levels (namely, 0.4%, 0.8%, 1.6% and 2.0%).

In Fig. 6, the down curves of the hysteresis loop of the paste without LS and those with 1.2% LS added by different addition methods (i.e., *SA*, *DA* and *PA*) are fitted by Bingham, Modified Bingham and Herschel-Bulkley models, respectively. It is evident that, for the reference mix (i.e., no LS), the fitted curves of the three rheological models are close to each other. However, in the presence of LS, the fitted curve of the Bingham model is slightly different from those of the other two non-linear models (i.e., Modified Bingham and Herschel-Bulkley). Furthermore, the differences of the fitted curves between the Bingham and the other two non-linear models are further enlarged by the separate addition of the SP and the activator (i.e., *DA* and *PA*). It can be easily noticed from Fig. 6 (c) and **(d)** that the regression curves of both non-linear models are better fitted than that of the Bingham model for *DA* and *PA*. A negative yield stress, which has no physical meaning, is only obtained by applying the Bingham model, indicating the error could occur with linear regression. To obtain a holistic understanding of the rheological behaviour of the LS-superplasticised SSASs, all the down curves of the pastes mixed by *SA, PA* and *DA* at the other LS dosages (namely, 0.4%, 0.8%, 1.6% and 2.0%) were also fitted into the Bingham, MB and HB models. The regression equations and R-squared values obtained from these analyses are listed and further compared in Table 3. Even though good regressions (as indicated by $R^2 > 0.96$) have been achieved by applying all the three rheological models, by adding the LS and the activator separately at different mix stages, a reduction in the R^2 value has occurred in the Bingham model, indicating that the reliability of the Bingham model for the separate addition methods has been reduced. By comparing the data in Table 3, it can be concluded that, instead of Bingham model, the MB model showed the best suitability for

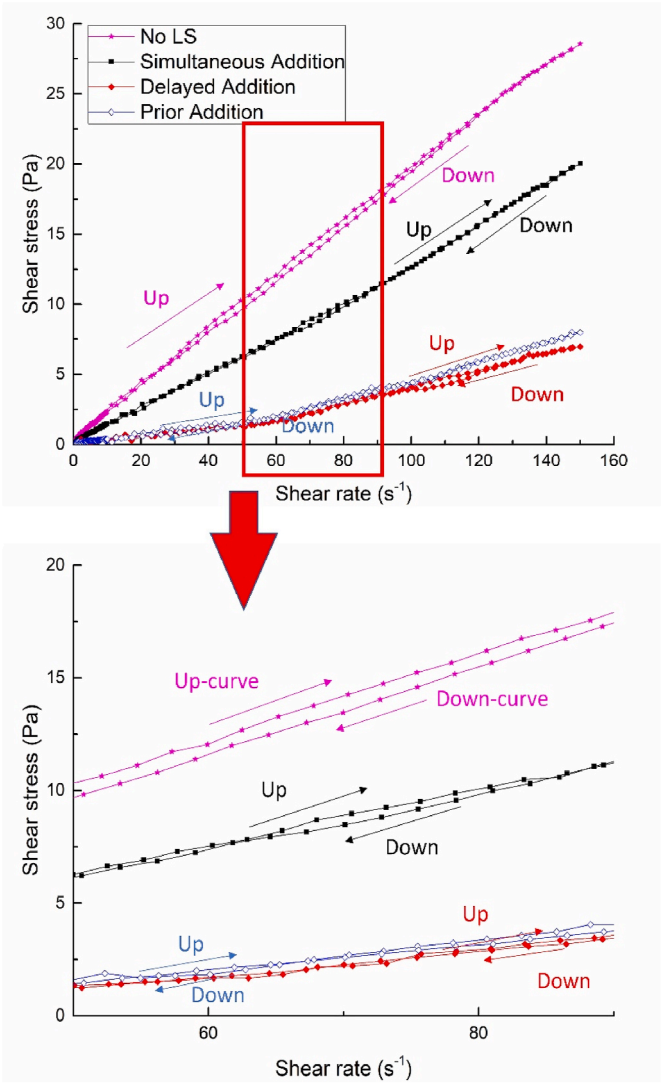

(a) flow curve SSAS with/without LS at 1.2% LS dosage

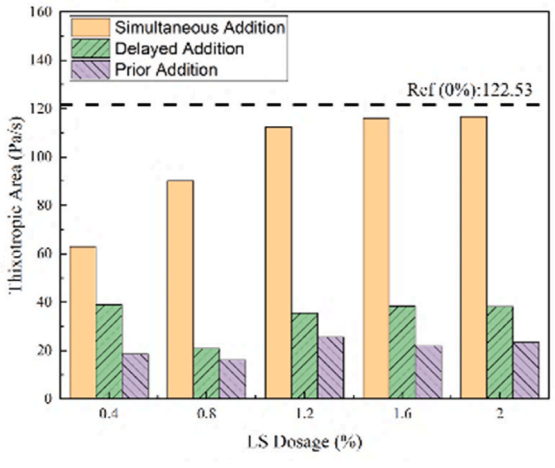

(b) thixotropic area of SSAS

Fig. 5. Thixotropic behaviour of SSAS pastes: (a) flow curve SSAS with/without LS at 1.2% LS dosage; (b) thixotropic area of SSAS.

describing the rheological behaviour of SSAS, in particular, the SSAS with LS SP. Similar trend has also be reported in self-compacting concrete by Fey et al. [42]. The possible reasons leading to this changed rheological behaviour, i.e., from Bingham to non-Bingham behaviour, will be discussed in Section 3.5 in the context of the observations made with ESEM.

3.2.2. Rheological parameter

Since a non-linear relationship between the shear stress and the shear rate was identified from all the mixes with separate additions of LS and activator, the rheological behaviour of the LS-superplasticised SSAS pastes are further compared using the rheological parameters, such as yield stress, plastic viscosity/consistence factor and exponent and c/μ, obtained from the Bingham (linear), Modified Bingham (non-linear) and Herschel-Bulkley (non-linear) models, whenever relevant, in this section below.

3.2.2.1. Yield stress. As shown in Figs. 7–9, in the presence of LS, the general trend is that the yield stresses of the LS-superplasticised SSAS pastes calculated from the Bingham (Fig. 7 (a)), Modified Bingham (Fig. 8 (a)) and Herschel-Bulkley models (Fig. 9 (a)) reduced with the increase of the LS dosage, especially when adding the LS and the activator separately at different mixing stages (i.e., both *DA* and *PA*). Compared to the *SA*, the separate addition methods significantly reduced the yield stress of the LS-superplasticised SSAS pastes, with the highest reduction being achieved by *PA* in all the three models. However, negative yield stresses from some of the mixes by *PA* and *DA* were observed from the Bingham model. As negative yield stress could not occur in reality, the suitability of the Bingham model for describing the rheological behaviour of the LS-superplasticised SSASs, in particular, when the LS is added by *DA* or *PA*, is thus, questionable [43]. Nonetheless, from the yield stress results, it could be anticipated that a better workability could be obtained from the separate addition methods, especially the *PA*. This is well corroborated by the minislump results presented in Fig. 3 and will be further discussed in Section 3.2.2.4 below.

3.2.2.2. Plastic viscosity and consistence factor. The effects of different LS addition methods on the plastic viscosity (based on Bingham model and MB model) of SSASs are plotted in Figs. 7 (b) and Fig. 8 (b), respectively. Apparently, increasing the LS dosage exhibited less effect on the reduction of plastic viscosity when the LS and the activator were added simultaneously. In fact, some slight increase in the plastic viscosity was even noticed from both the Bingham and the MB models with *SA* method. On the contrary, adding the LS and the activator separately at different mixing stages, the plastic viscosity was significantly decreased upon adding LS at a dosage of 0.4% in both models. However, there was no further reduction at the dosages above 0.4% and the difference between the *PA* and the *DA* was also insignificant. Nonetheless, the values of plastic viscosity were already very low (close to zero in both cases). On the other hand, the effects of different addition methods on the consistence factor (based on the HB model) were different. From Fig. 9 (b), it can be seen that there is no obvious trend for the consistence factor under *SA* when the SP dosage was increased. However, the consistence factors obtained from both *PA* and *DA* were lower than that from the *SA*, with an even slightly lower value being achieved from the *DA* when the dosage levels were below 1.2%. However, beyond 1.2%, a plateau was reached for both *PA* and *DA* and the change of LS dosage had no effect on the consistence factor thereafter. Again, very low values of consistence factors were achieved above 1.2% LS dosages.

3.2.2.3. Exponent and c/μ. The exponents from the HB model are plotted in Fig. 9 (c). It is clearly shown in the figure that the exponent of the reference paste (i.e., No LS) was around 1.0 and the addition of LS by *SA* had little effect on the exponent value. However, the exponent

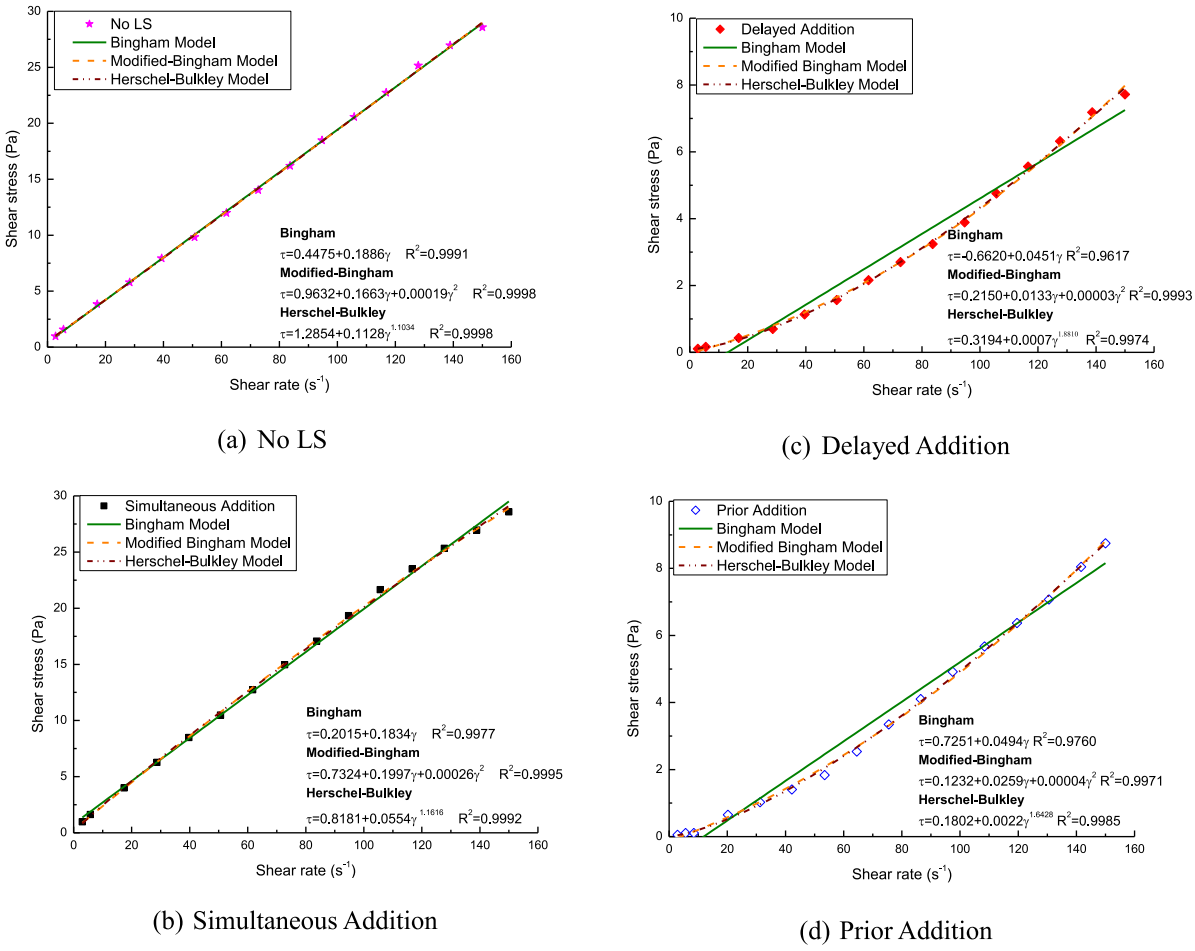

Fig. 6. Rheological models on flow curve (down curve) of SSAS with different LS addition.

Table 3
Regression analysis of the flow curves fitted by different rheological models.

Addition Method	SP Dosage	Bingham Model		Modified Bingham Model		Herschel-Bulkley Model	
		Equation	R^2	Equation	R^2	Equation	R^2
No LS	0	$\tau = 0.4475 + 0.1886\ \dot{\gamma}$	0.9991	$\tau = 0.9632 + 0.1663\ \dot{\gamma} + 1.8545E\text{-}04\dot{\gamma}^2$	0.9998	$\tau = 1.2854 + 0.1128\ \dot{\gamma}^{1.1034}$	0.9998
Simultaneous Addition	0.4%	$\tau = 0.3941 + 0.1768\ \dot{\gamma}$	0.9989	$\tau = 0.9054 + 0.1349\ \dot{\gamma} + 1.8192E\text{-}04\dot{\gamma}^2$	0.9998	$\tau = 0.7608 + 0.0860\ \dot{\gamma}^{1.1210}$	0.9998
	0.8%	$\tau = 0.3702 + 0.1982\ \dot{\gamma}$	0.9997	$\tau = 0.7560 + 0.1893\ \dot{\gamma} + 2.2713E\text{-}04\dot{\gamma}^2$	0.9997	$\tau = 0.7516 + 0.1381\ \dot{\gamma}^{1.0825}$	0.9993
	1.2%	$\tau = 0.2015 + 0.1834\ \dot{\gamma}$	0.9977	$\tau = 0.7324 + 0.1997\ \dot{\gamma} + 2.5648E\text{-}04\dot{\gamma}^2$	0.9995	$\tau = 0.8181 + 0.0554\ \dot{\gamma}^{1.1616}$	0.9992
	1.6%	$\tau = 0.1972 + 0.1951\ \dot{\gamma}$	0.9995	$\tau = 0.7127 + 0.1987\ \dot{\gamma} + 2.3653E\text{-}04\dot{\gamma}^2$	0.9998	$\tau = 0.8016 + 0.1358\ \dot{\gamma}^{1.0728}$	0.9998
	2.0%	$\tau = -0.0407 + 0.1973\ \dot{\gamma}$	0.9989	$\tau = 0.7115 + 0.1723\ \dot{\gamma} + 2.2574E\text{-}04\dot{\gamma}^2$	0.9998	$\tau = 0.7225 + 0.1782\ \dot{\gamma}^{1.0204}$	0.9997
Delayed Addition	0.4%	$\tau = 0.0698 + 0.0380\ \dot{\gamma}$	0.9601	$\tau = 0.5880 + 0.0153\ \dot{\gamma} + 3.7770E\text{-}05\dot{\gamma}^2$	0.9995	$\tau = 0.6815 + 0.0006\ \dot{\gamma}^{1.8601}$	0.9953
	0.8%	$\tau = -0.4944 + 0.0471\ \dot{\gamma}$	0.9665	$\tau = 0.2261 + 0.0147\ \dot{\gamma} + 3.3554E\text{-}05\dot{\gamma}^2$	0.9990	$\tau = 0.3062 + 0.0008\ \dot{\gamma}^{1.8461}$	0.9989
	1.2%	$\tau = -0.6620 + 0.0451\ \dot{\gamma}$	0.9617	$\tau = 0.2150 + 0.0133\ \dot{\gamma} + 3.0604E\text{-}05\dot{\gamma}^2$	0.9993	$\tau = 0.3194 + 0.0007\ \dot{\gamma}^{1.8810}$	0.9974
	1.6%	$\tau = -0.6132 + 0.0468\ \dot{\gamma}$	0.9694	$\tau = 0.1371 + 0.0127\ \dot{\gamma} + 2.9996E\text{-}05\dot{\gamma}^2$	0.9967	$\tau = 0.3830 + 0.0014\ \dot{\gamma}^{1.8339}$	0.9971
	2.0%	$\tau = -0.6234 + 0.0475\ \dot{\gamma}$	0.9765	$\tau = 0.1295 + 0.0119\ \dot{\gamma} + 2.7115E\text{-}05\dot{\gamma}^2$	0.9986	$\tau = 0.2530 + 0.0020\ \dot{\gamma}^{1.8558}$	0.9984
Prior Addition	0.4%	$\tau = 0.0558 + 0.0375\ \dot{\gamma}$	0.9753	$\tau = 0.5319 + 0.0264\ \dot{\gamma} + 4.8967E\text{-}05\dot{\gamma}^2$	0.9942	$\tau = 0.6075 + 0.0426\ \dot{\gamma}^{1.5744}$	0.9934
	0.8%	$\tau = -0.5403 + 0.0524\ \dot{\gamma}$	0.9840	$\tau = 0.1318 + 0.0242\ \dot{\gamma} + 4.4142E\text{-}05\dot{\gamma}^2$	0.9975	$\tau = 0.2804 + 0.0045\ \dot{\gamma}^{1.5025}$	0.9979
	1.2%	$\tau = -0.7251 + 0.0494\ \dot{\gamma}$	0.9760	$\tau = 0.1232 + 0.0259\ \dot{\gamma} + 4.5804E\text{-}05\dot{\gamma}^2$	0.9971	$\tau = 0.1802 + 0.0022\ \dot{\gamma}^{1.6428}$	0.9985
	1.6%	$\tau = -0.7254 + 0.0493\ \dot{\gamma}$	0.9721	$\tau = 0.1164 + 0.0226\ \dot{\gamma} + 4.0525E\text{-}05\dot{\gamma}^2$	0.9971	$\tau = 0.1771 + 0.0015\ \dot{\gamma}^{1.7182}$	0.9975
	2.0%	$\tau = -0.7868 + 0.0562\ \dot{\gamma}$	0.9750	$\tau = 0.0946 + 0.0205\ \dot{\gamma} + 4.1105E\text{-}05\dot{\gamma}^2$	0.9981	$\tau = 0.1345 + 0.0021\ \dot{\gamma}^{1.6793}$	0.9981

increased when the LS and the activator were added separately, indicating a shear thickening rheological behaviour could have occurred with both the *DA* and the *PA* methods, which will be further discussed in Section 3.5.

It should be noted that the MB model can be considered as an extension of the linear Bingham model with a second order term being introduced so that the nonlinear behaviour could be well described [14]. Therefore, as shown in Equation (4), there exists a theoretical relationship between c/μ (Fig. 8 (c)) and n (Fig. 9 (c)) [13]. From the data in Table 3, it is apparent that the c/μ values of all the pastes were positive, which was closely linked to the results of exponent obtained from the HB Model, indicating again that the shear thickening behaviour could have occurred in the LS-superplasticised SSAS.

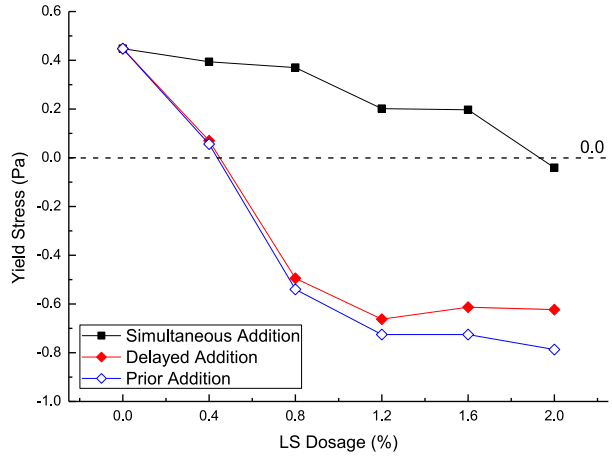

(a) Yield stress

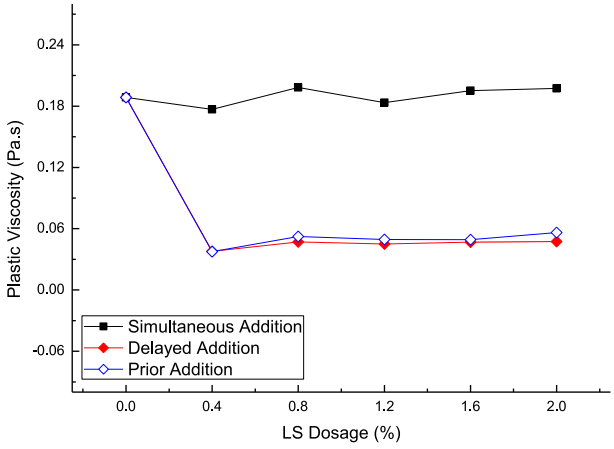

(b) Plastic viscosity

Fig. 7. Effect of LS dosage on the rheological properties of SSAS with different addition methods fitted by Bingham model.

$$\frac{c}{\mu}=\frac{1}{2a}\left(\frac{n-1}{2-n}\right) \tag{4}$$

Where: μ stands for plastic viscosity; a for random parameter; c for second order parameter, and n for exponent.

3.2.2.4. Relationship between minislump and rheological parameters. It has been well established by various researchers that a correlation exists between slump/minislump and yield stress [44]. To further verify the suitability of different rheological models for SSAS systems, the relationships between the yield stress obtained from the three different rheological models and the minislump spread of the SSASs are compared in Fig. 10. From the R^2 of the regression analysis, it can be seen that the highest R^2 was obtained from the MB model (0.9248 Vs 0.8773 from Bingham model and 0.8576 from Herschel-Bulkley Model), which indicates again that, among the three models, the MB model showed the best prediction of the workability by its yield stress. However, there is no relationship between the plastic viscosity (or consistence factor) and the minislump with the change of LS dosage (not shown in this paper) in the studied SSAS system, which is in agreement with those reported in PC systems [44].

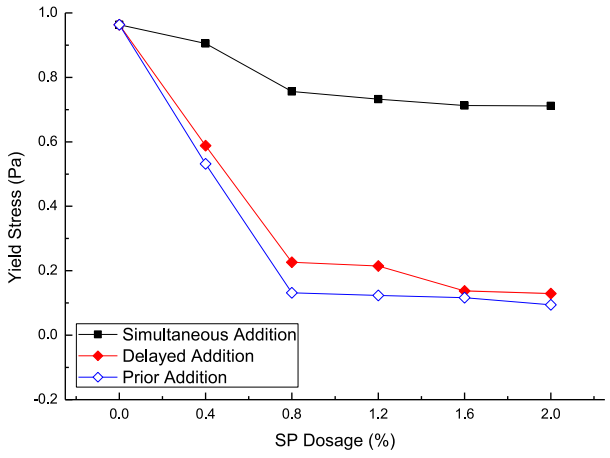

(a) Yield stress

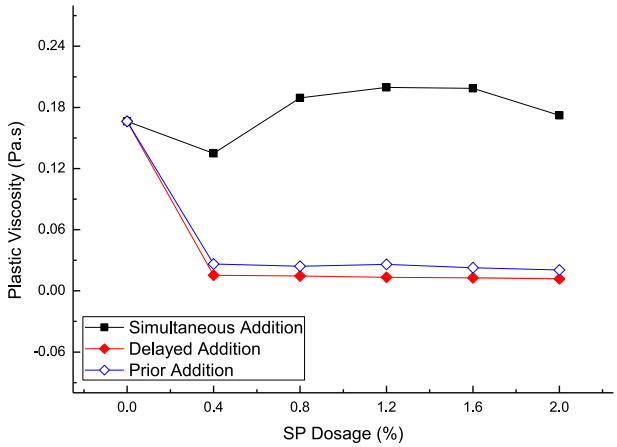

(b) Plastic viscosity

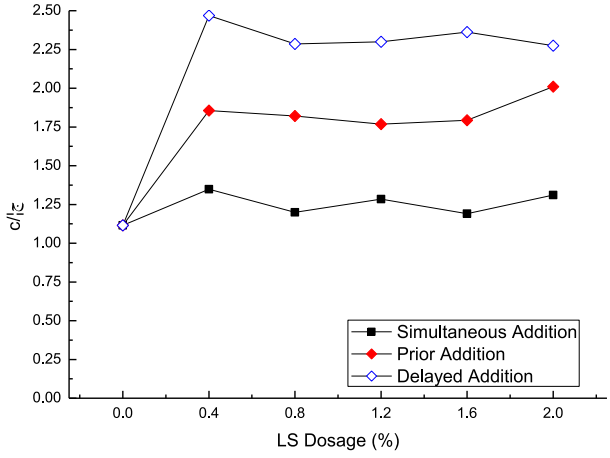

(c) c/μ value

Fig. 8. Effect of LS dosage on the rheological properties of SSAS with different addition methods fitted by Modified Bingham model.

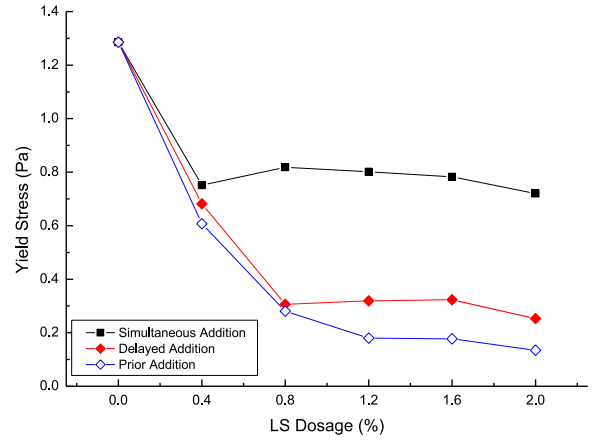

(a) Yield stress

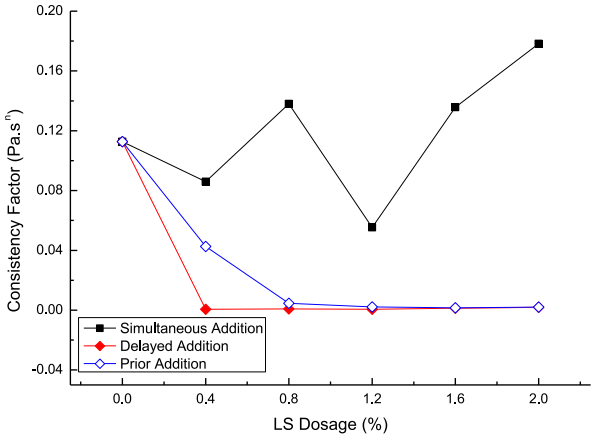

(b) Consistency

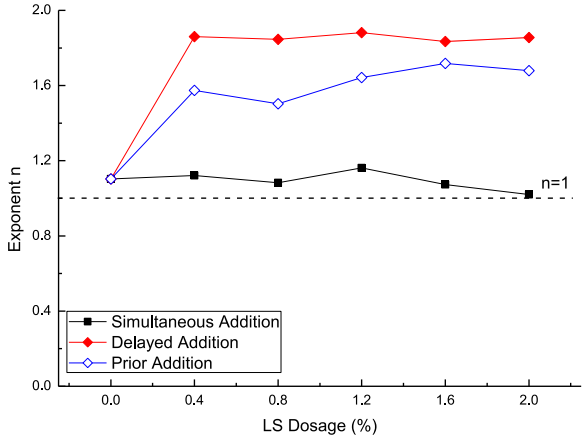

(c) Exponent

Fig. 9. Effect of LS dosage on the rheological properties of SSAS with different addition methods fitted by Herschel-Bulkley model.

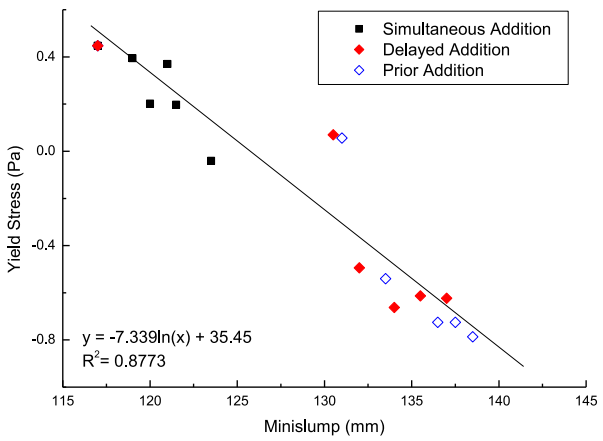

(a) Bingham model

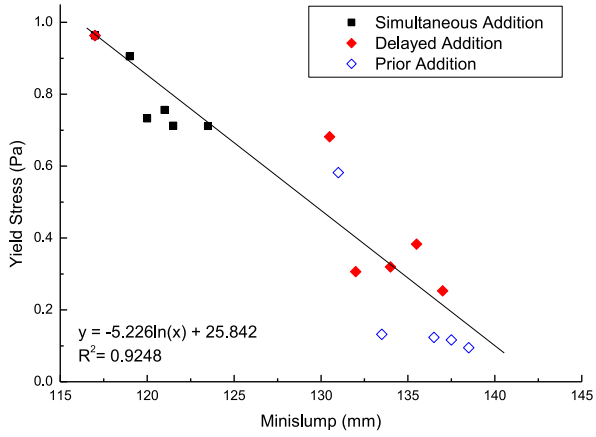

(b) Modified Bingham model

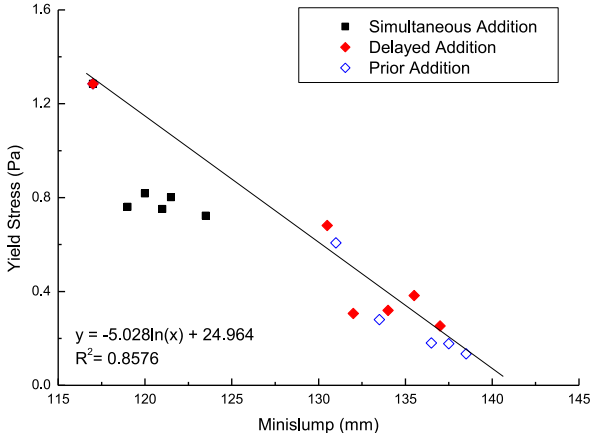

(c) Herschel-Bulkley model

Fig. 10. Relationship between initial minislump spread and yield stress calculated by different rheological model.

3.3. Adsorption isothermal

It is generally believed that the adsorption of the superplasticiser by hydrating cement particles is linked to the dispersion of cement particles in water. That is, the higher the adsorption of SP, the better the dispersion [45].The influence of the different addition methods on the adsorption of LS in SSAS was, thus, investigated and the results are shown in Fig. 11. It is evident from Fig. 11 that, compared with the mix

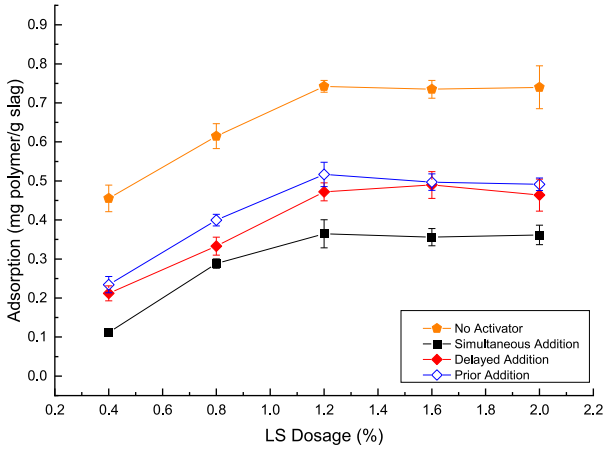

Fig. 11. Adsorption of LS in SSAS under different addition methods.

without the activator (i.e. the mix prepared with only slag and water, which was used as a control in the adsorption test for comparison purpose), the addition of activator by all the three methods (*SA, DA* and *PA*) resulted in a significant reduction in the adsorption of LS on the slag surface, which implies that either there is a competition between the activator and the LS during the adsorption to the slag surface or there are some adverse effects from the activator on the adsorption process of LS, or both [31,46]. Moreover, in the presence of the activator, compared with the simultaneous addition method at all dosage levels, the adsorptions of LS with both prior and delayed additions (i.e., *PA* and *DA*) were higher. It, thus, seems that the separate addition of the LS and the activator at different mixing stages can reduce the possible competition (if there are any) between the LS and the activator in adsorbing onto the surface of slag particles. This is, in particular, the case for the *PA* method, which might have provided a window (3 min) for the LS to play its dispersing role before the potential decomposition (if there are any) could have happened after the high alkaline activator is added. However, it should be noticed that, even for the *PA* method, the adsorption of the LS was still lower than that of the slag without activator, which suggests that the competitive adsorption and desorption from negatively charged sodium silicate activator could still have existed [46].

Fig. 11 also shows that the adsorbed amount of the LS increased rapidly with the increase of the LS dosages up to around 1.2% LS. At higher dosages (>1.2%), the adsorption increased slowly and gradually reached a plateau, following the trend of Langmuir isothermal adsorption. The quantitative analysis of the adsorption isothermal was, therefore, conducted using Langmuir adsorption (Equation (5)) and the results are presented in Table 4.

$$\frac{C}{A}=\frac{1}{A_S K}+\frac{1}{A_S}C \tag{5}$$

where C stands for equilibrium concentration of superplasticiser (LS in this study) (mg·L^{-1}), A for the adsorbed amount of superplasticiser by slag (mg·g^{-1}), A_s for the saturated adsorbed amount of superplasticiser (mg·g^{-1}) and K for the adsorption constant.

A linear relationship of C/A (g·L^{-1}) with C is normally observed with a regression coefficient close to one [47]. The A_s can be calculated by *1/slope* of the regressed straight lines, and constant K can be then obtained by *slope/intercept*. In this study, both the K and A_s were calculated and summarised in Table 4.

As can be seen from Table 4, when no activator was added, the highest A_s value (0.95 mg g^{-1}) was obtained which could be assumed that all the slag surface might have been occupied by LS. However, after the activator and the LS were added simultaneously (*SA*), the A_s values dropped by more than half and reached 0.43 mg g^{-1}, indicating that only less than half of the slag surface might have been occupied by the LS. This suggests that when the activator and the LS were added simultaneously, the activator was more prone to be adsorbed onto the surface of the slag. Compared to the *SA*, the characteristic plateau (A_s) of both the *PA* and the *DA* were increased from 0.43 mg g^{-1} (the A_s for SA) to 0.51 mg·g^{-1}and 0.46 mg g^{-1}, respectively. This implies that by adding the activator and the LS separately at different mixing stages, the adverse effect that the alkaline activator may have imposed on the adsorption of LS onto the slag surface could have been reduced. As a result, the relative amount of the LS adsorbed onto the slag surface was increased. However, it should be noted that the characteristic plateaus of *DA* and *PA* are 0.46 mg g^{-1} and 0.51 mg g^{-1}, respectively, suggesting that although both separate addition methods can reduce the adverse effect that the alkaline activator might have imposed on the adsorption of LS onto slag, *PA* is more effective than *DA*. Consequently, it can be deduced that the workability of SSAS with *PA* should be better than *DA* and *SA*, which is well supported by the minislump results presented in Fig. 3.

As illustrated in Fig. 12, although it is difficult to establish a quantitative relationship between the adsorbed LS and the minislump value for all the three addition methods, separate trends can be identified for *SA* and (*DA* + *PA*) respectively, indicating that different mechanisms might be functioning in *SA* and (*DA* + *PA*). Nonetheless, regardless of the possible mechanism involved, it still can be seen that, in general, a higher adsorbed amount of LS fosters a better workability of SSAS. Moreover, at similar adsorption of LS, the minislumps of the SSAS pastes produced by the separate addition methods, i.e., *DA* and *PA*, were higher than that from *SA*. This could be attributed to the reduction of the possible competitive adsorption as well as the improved chemical stability of the LS due to the separate addition of the SP and the activator [48]. As reported by Palacios and Puertas [27], the SPs designed for Portland Cement are not chemically stable in highly alkaline sodium silicate solution, and could result in the loss of surface activity. This might be the reason that adding SPs simultaneously with alkaline

Table 4
Adsorption characteristics of the LS in SSAS with different addition methods.

Activator	Addition method	R^2	Slope	Intercept/ g·L^{-1}	k/ L·g^{-1}	A_s/ mg·g^{-1}
None	N/A	0.96	1056.07	1044.73	0.85	0.95
Sodium Silicate	Prior Addition (PA)	0.99	1955.39	1089.06	1.80	0.51
	Simultaneous Addition (SA)	0.98	2339.25	1015.03	2.30	0.43
	Delayed Addition (DA)	0.99	2178.85	1072.55	2.03	0.46

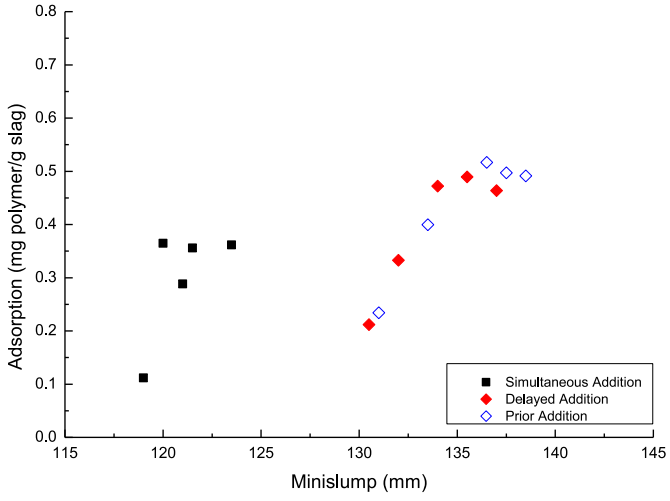

Fig. 12. Relationship between adsorption and minislump of SSAS.

activator (i.e., *SA*) is not suitable for alkali-activated cementitious materials (AACM) because in this method the SP is directly mixed with the alkaline activator, which could lead to the loss of surface activity of SP. On the contrary, in the case of separate addition of SP and activator (such as *DA* and *PA*), the SP is exposed to a less alkaline environment, which could potentially reduce or even prevent the interaction between the SP and the activator and, hence, improve the performance of SP in AACM. The result obtained from the LS-superplasticised SSAS in the current study is just a good example to exemplify this hypothesis. Nonetheless, similar to what has already been reported in PC system, separate addition of SP and activator, in turn, could lead to different rheological behaviour of the AACM, as, again, exemplified by the rheological behaviour of the LS-superplasticised SSAS reported in this study.

3.4. Zeta potential

Zeta potential is the potential at the shear plane between the suspended solid particles and the liquid phase [49], which has often been used to describe the interactions between the particles and the superplasticisers in cement research [50]. Generally, it is believed that a higher absolute zeta potential value is linked to a better dispersion (and, hence, a lower yield stress) between solid particles and an increased workability [51].

The results of the zeta potential of SSAS pastes are shown in Fig. 13. As can be seen, in the absence of LS, the zeta potential of SSAS was close to −47.3 mV whereas the 'pure' slag mix (i.e., the slag was only mixed with water without adding sodium silicate) only showed a zeta potential of around −15 mV.

When slag is mixed with water, it is expected that a basic pH environment could be formed [52]. As a result, some sillanol groups on the slag surface could deprotonate and, thus, induce a net negatively charged surface. With further dissolution of the alkali and earth alkali cations from slag into the solution under this alkaline environment, cationic species such as Na^+, K^+ and Ca^{2+}, will then be released into the solution. However, since the rate of the dissolution of these cationic ions is faster than that of their diffusion, some cationic species, in particular, Ca^{2+}, could accumulate and then be adsorbed onto the surface of the deprotonated silanol groups, introducing some positively charged sites in the double-layered structure [53]. This may explain why the initially formed negative zeta potential is observed to shift to less negative and sometimes even slightly positively zeta potential over time [54]. In the current study, a −15mV has been measured from pure slag mix which is similar to those reported in the literature [55]. When sodium silicate solution is added into the slag mix (i.e., without adding the LS), not only the surface reaction similar to the pure slag mix (i.e., slag/water mix) could occur, a more intense surface reaction is also to be anticipated due to the strong alkaline environment introduced by sodium silicate solution. As a result, one may expect that more cationic species, such as Na^+, K^+ and Ca^{2+}, could be released from the slag surface into the solution and then adsorbed onto the surface of the slag particles. Consequently, a more positive zeta potential value should have been anticipated [54]. In contrast, a more negative, i.e., - 47.3 mV, zeta potential was measured in this study when sodium silicate solution was added, which indicates that, as a strong electrolyte, sodium silicate itself has more influence on the surface charge of slag [55]. This is mainly due to the fact that the negatively charged silicate species from sodium silicate can also adsorb or precipitate onto the surface of slag particles, leading to a more negative zeta potential value, overriding its activation effects on slag. Similar results have also been reported by Kashani et al. [55].

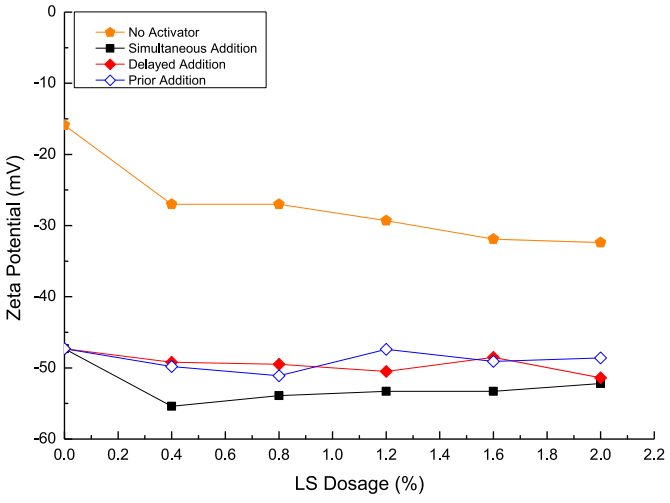

Fig. 13. Zeta potential of LS in SSAS under different addition methods.

When the LS was added into the 'pure' slag mix (i.e., without activator), a further reduction of the zeta potential can be observed in Fig. 13 and, in general, the zeta potential was decreased with the increase of the LS dosages. For example, with 1.2% LS being added, the zeta potential of the slag without activator was reduced from −15 mV to around −29 mV and this was then becoming almost stable, which is similar to the pattern observed from the adsorption results in Fig. 11. Therefore, the increased absolute value of the zeta potential (i.e., more negative) might be attributed to the higher amount of LS adsorbed onto the surface of slag particles. As highlighted before, when the slag is dispersed in water, depending on the type of slag, a significant amounts of the cations, i.e., Ca^{2+}, Mg^{2+}, K^+ and Na^+, are released during the dissolution process [54] and these cations can adsorb onto the negatively charged silanol groups on the surface of the slag particles, introducing some positively charged sites. Since the LS in hydrolysed form is a type of negatively charged polymer, once dissolved in water the LS could then be adsorbed onto the surface of the slag via the electrostatic attraction to the cations that have already adsorbed onto the surface of slag particles, leading to a further decreased zeta potential (i.e., more negative) of the LS-superplasticised slag.

However, when the LS was added into the SSASs, regardless of the addition methods, the reduction in the zeta potential was less significant and the reduction pattern as observed in the LS-superplasticised 'pure' slag mix was missing. Considering the fact that a zeta potential of −47.3 mV and a range of zeta potentials between −25 mV and −30 mV have been developed by the pure SSAS and the LS-superplasticised slags (i.e., no activator), respectively, it becomes immediate obvious from Fig. 13 that, the combination of the activator and the LS is not just a simple superimposition of the zeta potentials of these two. Additionally, it can be noticed from the same figure that the zeta potential trend of the LS-superplasticised SSASs cannot be correlated with the Langmuir isothermal adsorption pattern presented in Fig. 11. As it is generally accepted that a higher superplasticiser adsorption should result in a higher zeta potential [31], the contradicting results between the adsorption in Fig. 11 and the zeta potential in Fig. 13 in the current study would indicate that some interactions could have happened between the LS and the sodium silicate solution. Because of these interactions, it has made it rather complex and almost impossible to correlate the zeta potential with the LS adsorption as well as the rheology of SSAS results as reported before. Consequently, it becomes impossible to make use of the zeta potential data to interpret the possible mechanisms involved when different LS addition methods were adopted in this study. For example, it can be seen from Fig. 13 that, compared with the *SA*, even though the absolute values of the zeta potential of SSASs under both separate addition methods were decreased (i.e. moving towards more positive direction), instead of leading to a higher yield stress (and reduced workability), it has actually resulted in a lower yield stress (shown in Fig. 7) and a better workability (shown in Fig. 3), which just contradicts to the commonly accepted theory [56]. Although further research is still needed before the exact nature of these interactions can be fully understood, the complicated structure of sodium silicate micelle should

have, at least, partly contributed to this complex [57,58]. Furthermore, due to this complex nature, one cannot simply interpret the zeta potential results by just considering the effect of LS and activator separately. A synergistic effect from both sodium silicate solution and the LS has to be considered.

3.5. ESEM

The effect of different addition methods on the dispersion of slag particles in SSAS mixes was further investigated by ESEM, and the selected images of the SSAS at 10 min after mixing are shown in Fig. 14. However, as the ESEM images can only provide qualitative information based on visual observation, a judgement on the dispersion of slag particles fully based on ESEM images could, thus, be subjective. To identify the exact effect that different addition methods may have on the dispersion of slag particles, a more objective method is preferred. In this study, the ESEM images shown in Fig. 14 were, therefore, quantitatively analysed by ImageJ [59] and the resulting particle size (i.e., Heywood diameter of slag particles) distributions and cumulative curves of the slag particles are presented in Fig. 15.

As can be seen from Fig. 15(a), without adding LS, there exists a considerable number of agglomerates of slag particles in 'pure' SSAS (i.e., SSAS without adding LS). This observation is further confirmed by the particle size distribution obtained by ImageJ in Fig. 15 which clearly showed that the portion of larger particles in SSAS without LS is higher than that of the SSASs with LS under different addition methods. For example, when the Heywood diameter is $\geq$ 10 μm, the SSAS without LS showed the highest proportion of particles among the SSASs investigated. In contrast, when the Heywood diameter is $<$ 5 μm, the SSASs without LS showed smaller proportion of particles. As discussed previously, the addition of sodium silicate activator into slag could increase the complexity of the surface chemistry environment of slag due to the further released alkali and earth alkali cations as well as the increased electrostatically counter silanol groups [55] generated from the accelerated dissolution of slag under this strong alkaline environment. Moreover, the quick formation of some initially precipitated hydration products could have also affected the dispersion of SSAS [68]. Therefore, it is generally agreed that, compared to PC, AAS usually exhibits a poor workability [28]. Furthermore, as presented in Fig. 5(b), the 'pure' SSAS showed the largest thixotropic area, which can also be used to verify this observation because it has already indicated that there should exist some flocculation of slags.

However, when the LS was added into the SSASs, regardless of its addition methods, less agglomerates and better dispersion of the slag particles was, in general, observed (Fig. 14 (b), (c) and (d)), which implies that LS can improve the dispersion of slag particles even in a highly alkaline media. As shown in Fig. 15(a), compared to the 'pure' SSAS, higher portion of small particles with Heywood diameter <5 μm, whilst less portion of large particle with Heywood diameter >15 μm, was observed in SSASs with LS. This results was further confirmed by Fig. 15

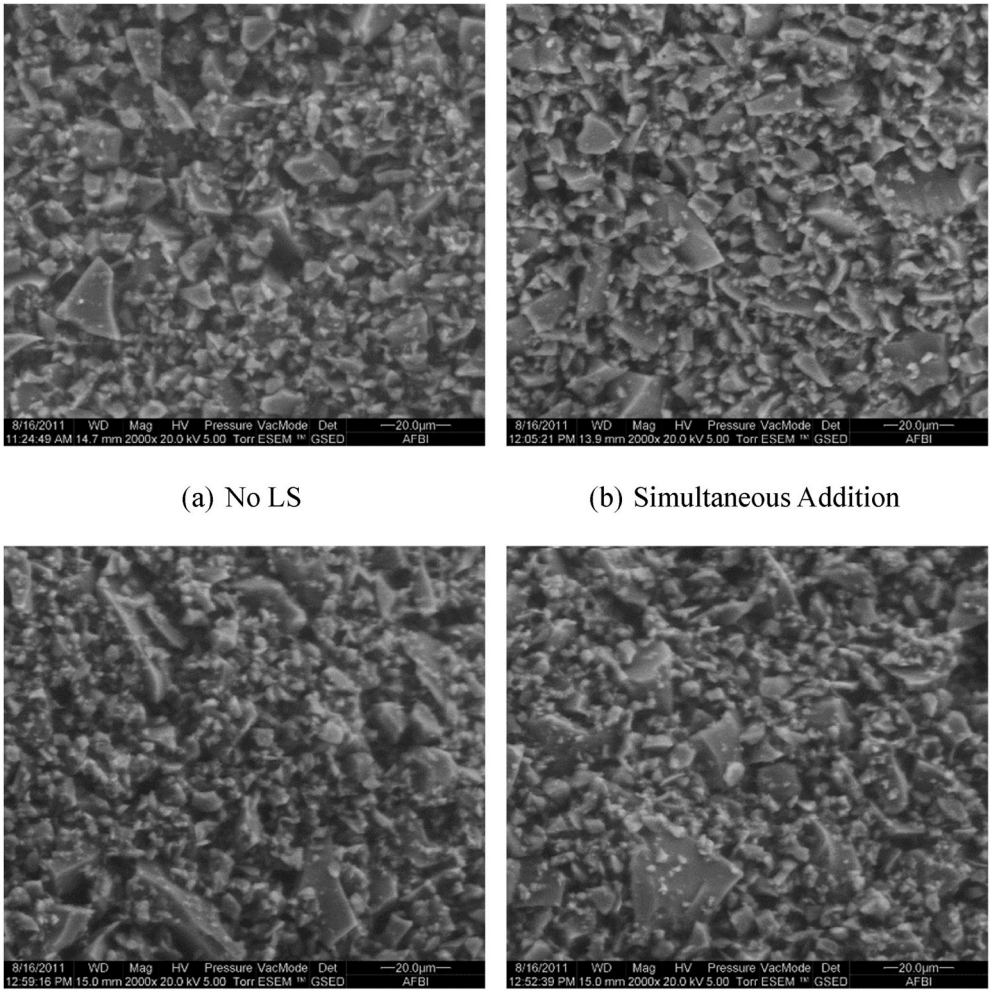

Fig. 14. Selected ESEM image of SSAS with different LS addition methods (1.2% LS dosage by the mass of slag).

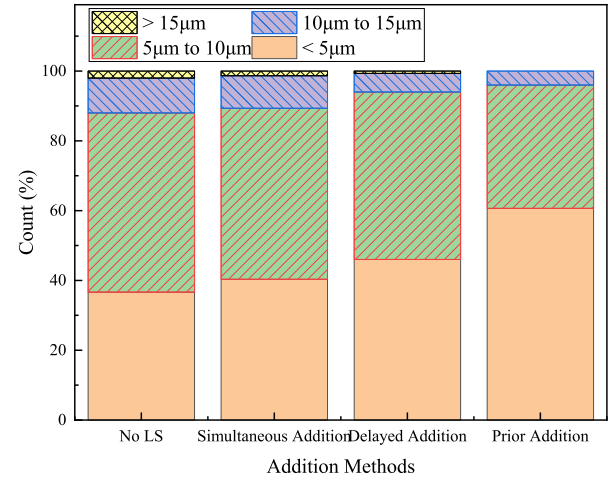

(a) Particle size distribution of slag

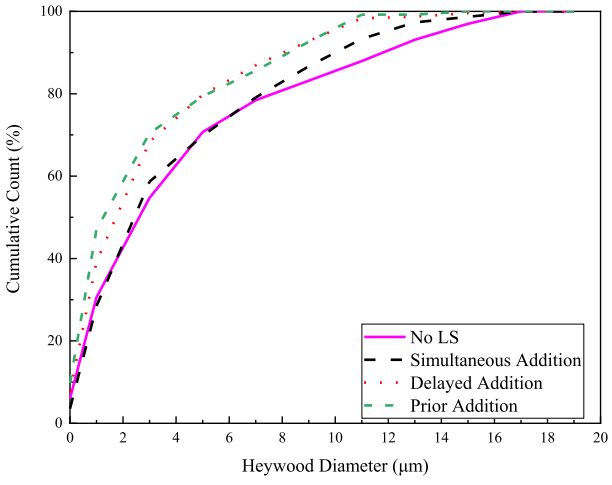

(b) Cumulative curve of slag particles

Fig. 15. Particles size (Heywood Diameter) distribution and cumulative curve of SSAS with different LS addition methods from ESEM image.

(b), in which the particle size distribution curves of SSASs with LS all shifted to left of the 'pure' SSAS, suggesting that more small particles exist in the SSASs with LS. This observation also correlates well with the increased minislump and decreased yield stress of the LS-superplasticised SSAS in Fig. 3 and Figs. 7(a), 8(a) and 9(a), respectively. Since LS is a highly cross-linked polymer, consisting of various phenyl-propanoid units with coniferyl alcohol, sinapyl alcohol and *p*-coumaryl identified as three main components [60], when it is hydrolysed, a negatively charged backbone and countering cations can be formed. As a result, electrostatic repulsion has been considered as the dominant dispersion mechanism. Although the deteriorated SP performance in AAS has been reported by various researchers [61–64], which was primarily attributed to the cleavage of some functional groups of the SPs, the current results would suggest that not all the functional groups are unstable in alkaline environment and, hence, the addition of LS still can increase the dispersion of SSAS [48].

Furthermore, as anticipated, out of the three addition methods, less agglomerates were observed in the SSAS pastes prepared by both *DA* and *PA* (as shown in Fig. 14 (c) and (d), respectively) as compared to that of *SA* (Fig. 14 (b)). In addition, as can be seen in Fig. 14 (a), the largest portion of particles was obtained from the Heywood diameter <5 μm under *PA*, indicating that the best dispersion was achieved from *PA* among those three addition methods. This observation again correlates very well with the results presented in Fig. 5 (b), which showed that regardless of the LS dosages, the smallest thixotropic area was obtained under *PA*. Furthermore, the observation from Fig. 14 can also be corroborated by the adsorption results presented in Fig. 11 where *PA* also showed the highest LS adsorption out of the three different addition methods which again is expected to show the best dispersion of slag particles [31].

To conclude, based on the ESEM observation as well as the quantitative analysis by ImageJ, it is evident that better dispersion of slag particles can be achieved from the separate addition of LS and alkaline activator. In particular, the best is achieved by the *PA* method (i.e., adding LS 3 min before activator), which is believed to be due to the reduced competition in adsorption between LS and alkaline activator as well as the increased stability of the LS prior to the inclusion of alkaline activator in the SSASs [48]. It has been well-established that the presence of sufficient amounts of small particles is one of the prerequisite conditions for the occurrence of shear thickening behaviour [65]. Therefore, the shear thickening behaviour observed in this paper when LS and alkaline activator were added separately is mainly attributed to the improved dispersion of the slag particles as clearly showed in Figs. 14 and 15. This is because, in theory, a shear thickening behaviour could occur under two conditions, namely, high-volume fraction of the solids and non-flocculated particles [11]. Under such a circumstance, when the hydrodynamic forces overcome the repulsive forces, such as the electrostatic force, Brownian force and steric force [65,66], temporary agglomerates can be formed. As a result, shear thickening could occur as the viscosity increases with increasing shear rate due to the enlargement of the particle clusters [67].

4. Conclusions

Based on the results presented in this paper, the following conclusions can be drawn:

1) Both the initial workability and the 60-min minislump retention of lignosulfonate-superplasticised SSAS (in term of the minislump) can be effectively improved by separate addition of LS and alkaline activator at the different stages of mixing. Furthermore, the prior addition of LS has demonstrated even better workability than the delayed addition of LS. Therefore, the separate addition of LS and alkaline activator at different mixing stages could be a simple and effective approach to tackle the incompatibility issue of applying PC based SPs in alkali-activated slag.
2) Separate LS addition methods changed the linear rheological behaviour of SSAS to non-linear. As a result, the Bingham model is no longer the best rheological model for the SSAS systems when LS and alkaline activator are added separately. Through a detailed analysis presented in this paper, the Modified Bingham has been identified as the best model for describing the rheological behaviour of lignosulfonate-superplasticised SSAS.
3) The addition of LS increased the magnitude of the zeta potential of SSAS. However, compared to the simultaneous addition of LS and alkaline activator, the magnitude of zeta potential of SSAS decreased by both prior and delayed addition methods, even though the workability and rheological behaviour of lignosulfonate-superplasticised SSASs were improved. This observation contradicts to the commonly accepted theory, although it could be presumably attributed to the complicated structure of sodium silicate micelle. Further research is therefore still needed to investigate the synergistic effect of sodium silicate activator and LS on the SSASs before the fundamental mechanisms behind the rheological behaviour observed in the current study could be fully understood.

Declaration of competing interest

The authors declare that they have no known competing financial interests or personal relationships that could have appeared to influence the work reported in this paper.

Data availability

Data will be made available on request.

Acknowledgement

Dr Jun Ren was previously sponsored by an International PhD studentship in Queen's University Belfast and an International PhD studentship in University College London. Dr Martyn J. Earle from The Queen's University Ionic Liquid Laboratories, Queen's University Belfast, U.K. is specially appreciated for his kind support. The financial supports from the UK-China Bridge in Sustainable Energy and Built Environment (UC-SEBE) (EP/G042594/1) and National Natural Science Foundation of China (Grant No. 52168038, 51908526) are also grateful acknowledged.

References

[1] M.K. Rahman, M.H. Baluch, M.A. Malik, Thixotropic behavior of self compacting concrete with different mineral admixtures, Construct. Build. Mater. 50 (2014) 710–717.
[2] O.H. Wallevik, D. Feys, J.E. Wallevik, K.H. Khayat, Avoiding inaccurate interpretations of rheological measurements for cement-based materials, Cement Concr. Res. 78 (2015) 100–109.
[3] P.F.G. Banfill, M.A.O.M. Teixeira, R.J.M. Craik, Rheology and vibration of fresh concrete: predicting the radius of action of poker vibrators from wave propagation, Cement Concr. Res. 41 (2011) 932–941.
[4] J.A. Lewis, H. Matsuyama, G. Kirby, S. Morissette, J.F. Young, Polyelectrolyte effects on the rheological properties of concentrated cement suspensions, J. Am. Ceram. Soc. 83 (2000) 1905–1913.
[5] H.A. Barnes, K. Walters, The yield stress myth? Rheol. Acta 24 (1985) 323–326.
[6] G. Gelardi, R.J. Flatt, 11 - working mechanisms of water reducers and superplasticizers, in: P.-C. Aïtcin, R.J. Flatt (Eds.), Science and Technology of Concrete Admixtures, Woodhead Publishing, 2016, pp. 257–278.
[7] N. Roussel, G. Ovarlez, S. Garrault, C. Brumaud, The origins of thixotropy of fresh cement pastes, Cement Concr. Res. 42 (2012) 148–157.
[8] L.J. Struble, W.G. Lei, Rheological changes associated with setting of cement paste, Adv. Cement Base Mater. 2 (1995) 224–230.
[9] D. Feys, R. Verhoeven, G. De Schutter, Fresh self compacting concrete, a shear thickening material, Cement Concr. Res. 38 (2008) 920–929.
[10] F. Larrard, C.F. Ferraris, T. Sedran, Fresh concrete: A Herschel-Bulkley material, Mater. Struct. 31 (1998) 494–498.
[11] M. Cyr, C. Legrand, M. Mouret, Study of the shear thickening effect of superplasticizers on the rheological behaviour of cement pastes containing or not mineral additives, Cement Concr. Res. 30 (2000) 1477–1483.
[12] V.H. Nguyen, S. Remond, J.L. Gallias, Influence of cement grouts composition on the rheological behaviour, Cement Concr. Res. 41 (2011) 292–300.
[13] D. Feys, R. Verhoeven, G. De Schutter, Evaluation of time independent rheological models applicable to fresh Self-Compacting Concrete, Appl. Rheol. 17 (2007), 56244-56241-56244-56210.
[14] H. Güllü, Comparison of rheological models for jet grout cement mixtures with various stabilizers, Construct. Build. Mater. 127 (2016) 220–236.
[15] C. Shi, P.V. Krivenko, D. Roy, Alkali-activated Cements and Concretes, Spons Architecture Price Book, 2006.
[16] Q. Ma, S.V. Nanukuttan, P.A.M. Basheer, Y. Bai, C. Yang, Chloride transport and the resulting corrosion of steel bars in alkali activated slag concretes, Mater. Struct. 49 (2016) 3663–3677.
[17] A.M. Rashad, Y. Bai, P.A.M. Basheer, N.C. Collier, N.B. Milestone, Chemical and mechanical stability of sodium sulfate activated slag after exposure to elevated temperature, Cement Concr. Res. 42 (2012) 333–343.
[18] J. Liu, L. Hu, L. Tang, J. Ren, Utilisation of municipal solid waste incinerator (MSWI) fly ash with metakaolin for preparation of alkali-activated cementitious material, J. Hazard Mater. 402 (2021), 123451.
[19] J. Ren, L. Hu, Z. Dong, L. Tang, F. Xing, J. Liu, Effect of silica fume on the mechanical property and hydration characteristic of alkali-activated municipal solid waste incinerator (MSWI) fly ash, J. Clean. Prod. 295 (2021), 126317.
[20] K. Yang, C. Yang, J. Zhang, Q. Pan, L. Yu, Y. Bai, First structural use of site-cast, alkali-activated slag concrete in China, Proceedings of the Institution of Civil Eng. Struct. Build. 171 (2018) 800–809.
[21] Y. Bai, N.C. Collier, N.B. Milestone, C.H. Yang, The potential for using slags activated with near neutral salts as immobilisation matrices for nuclear wastes containing reactive metals, J. Nucl. Mater. 413 (2011) 183–192.
[22] A. Gruskovnjak, B. Lothenbach, L. Holzer, R. Figi, F. Winnefeld, Hydration of alkali-activated slag: comparison with ordinary Portland cement, Adv. Cement Res. 18 (2006) 119–128.
[23] X. Hu, C. Shi, X. Liu, Z. Zhang, Studying the effect of alkali dosage on microstructure development of alkali-activated slag pastes by electrical impedance spectroscopy (EIS), Construct. Build. Mater. 261 (2020), 119982.
[24] Q. Li, K. Yang, C. Yang, An alternative admixture to reduce sorptivity of alkali-activated slag cement by optimising pore structure and introducing hydrophobic film, Cement Concr. Compos. 95 (2019) 183–192.
[25] M. Palacios, P.F.G. Banfill, F. Puertas, Rheology and setting of alkali-activated slag pastes and mortars: effect of organ admixture, ACI Mater. J. 105 (2008) 140–148.
[26] F. Puertas, C. Varga, M.M. Alonso, Rheology of alkali-activated slag pastes. Effect of the nature and concentration of the activating solution, Cement Concr. Compos. 53 (2014) 279–288.
[27] M. Palacios, F. Puertas, Stability of Superplasticizer and shrikage-reducing admixtures in high basic media, Mater. Construcción 54 (2004) 65–86.
[28] M. Palacios, F. Puertas, Effect of superplasticizer and shrinkage-reducing admixtures on alkali-activated slag pastes and mortars, Cement Concr. Res. 35 (2005) 1358–1367.
[29] J.L. Provis, J.S.J.V. Deventer, Alkali Activated Materials: State-Of-The-Art Report, RILEM TC 224-AAM, 2013.
[30] T. Bakharev, J.G. Sanjayan, Y.B. Cheng, Effect of admixtures on properties of alkali-activated slag concrete, Cement Concr. Res. 30 (2000) 1367–1374.
[31] M. Palacios, Y.F. Houst, P. Bowen, F. Puertas, Adsorption of superplasticizer admixtures on alkali-activated slag pastes, Cement Concr. Res. 39 (2009) 670–677.
[32] J. Ren, Y. Bai, M.J. Earle, C.H. Yang, Effect of Different Addition Methods of Lignosulfonate Admixture on the Adsorption, Zeta Potential and Fluidity of Alkali-Activated Slag Binder, Young Researchers' Forum in Construction Materials London, 2012.
[33] I. Aiad, S. Abd El-Aleem, H. El-Didamony, Effect of delaying addition of some concrete admixtures on the rheological properties of cement pastes, Cement Concr. Res. 32 (2002) 1839–1843.
[34] M. Sonebi, M.T. Bassuoni, J. Kwasny, A.K. Amanuddin, Effect of nanosilica on rheology, fresh properties, and strength of cement-based grouts, J. Mater. Civ. Eng. 27 (2015), 04014145.
[35] P.F.G. Banfill, G. Starrs, G. Derruau, W.J. McCarter, T.M. Chrisp, Rheology of low carbon fibre content reinforced cement mortar, Cement Concr. Compos. 28 (2006) 773–780.
[36] A. Papo, L. Piani, Effect of various superplasticizers on the rheological properties of Portland cement pastes, Cement Concr. Res. 34 (2004) 2097–2101.
[37] G. Venkiteela, Z. Sun, In situ observation of cement particle growth during setting, Cement Concr. Compos. 32 (2010) 211–218.
[38] R. Kumari, N. Rana, Particle size and shape analysis using imagej with customized tools for segmentation of particles, Int. J. Eng. Res. 4 (2015).
[39] S.W. Kim, Effect of particle size on carbon nanotube aggregates behavior in dilute phase of a fluidized bed, Processes 6 (2018) 121.
[40] M. Chen, L. Yang, Y. Zheng, Y. Huang, L. Li, P. Zhao, S. Wang, L. Lu, X. Cheng, Yield stress and thixotropy control of 3D-printed calcium sulfoaluminate cement composites with metakaolin related to structural build-up, Construct. Build. Mater. 252 (2020), 119090.
[41] E. Koehler, S. Amziane, V. Bui, Y. Deshpande, R. Ferron, J. Hu, Z. Li, M. Nehdi, R. Pileggi, J. Tanesi, D. Beaupre, S.E. Chidiac, P. Domone, D. Fowler, A. Kappi, R. McCarthy, H. Ozyildirim, K. Sobolev, K. Wang, M.-H. Zhang, ACI 238.2T-14 TechNote Concrete Thixotropy, american concrete institute technote, ACI 238 (2014) 2T–14T.
[42] D. Feys, J.E. Wallevik, A. Yahia, K.H. Khayat, O.H. Wallevik, Extension of the Reiner–Riwlin equation to determine modified Bingham parameters measured in coaxial cylinders rheometers, Mater. Struct. 46 (2013) 289–311.
[43] J. Ren, Y. Bai, M.J. Earle, C.H. Yang, A Preliminary Study on the Effect of Separate Addition of Lignosulfonate Superplasticiser and Waterglass on the Rheological Behaviour of Alkali-Activated Slags, Third International Conference on Sustainable Construction Materials & Technologies, SCMT3)Kyoto, 2013.
[44] J.E. Wallevik, Relationship between the Bingham parameters and slump, Cement Concr. Res. 36 (2006) 1214–1221.
[45] R.J. Flatt, Y.F. Houst, A simplified view on chemical effects perturbing the action of superplasticizers, Cement Concr. Res. 31 (2001) 1169–1176.
[46] C.H. Yang, Y. Song, K. Chen, J.X. Ye, A. Jiang, Adsorption characteristics of surfactant in alkali- activated slag cement systems, Concrete (2009) 42–45.
[47] Q.P. Ran, P. Somasundaran, C.W. Miao, J.P. Liu, S.S. Wu, J. Shen, Adsorption mechanism of comb polymer dispersants at the cement/water interface, J. Dispersion Sci. Technol. 31 (2010) 790–798.
[48] J. Ren, Superplasticiser for NaOH-Activated Slag: Competition and Instability between Superplasticiser and Alkali-Activator, Department of Civil, Environmental and Geomatic Engineering, University College London, 2016.
[49] E. Nägele, The zeta-potential of cement, Cement Concr. Res. 15 (1985) 453–462.
[50] A. Zingg, F. Winnefeld, L. Holzer, J. Pakusch, S. Becker, L. Gauckler, Adsorption of polyelectrolytes and its influence on the rheology, zeta potential, and microstructure of various cement and hydrate phases, J. Colloid Interface Sci. 323 (2008) 301–312.
[51] J. Gustafsson, P. Mikkola, M. Jokinen, J.B. Rosenholm, The influence of pH and NaCl on the zeta potential and rheology of anatase dispersions, Colloids Surf. A Physicochem. Eng. Asp. 175 (2000) 349–359.
[52] D. Ménétrier, I. Jawed, T.S. Sun, J. Skalny, ESCA and SEM studies on early C3S hydration, Cement Concr. Res. 9 (1979) 473–482.

[53] A. Habbaba, J. Plank, Surface chemistry of ground granulated blast furnace slag in cement pore solution and its impact on the effectiveness of polycarboxylate superplasticizers, J. Am. Ceram. Soc. 95 (2012) 768–775.
[54] A. Habbaba, J. Plank, Interaction between polycarboxylate superplasticizers and amorphous ground granulated blast furnace slag, J. Am. Ceram. Soc. 93 (2010) 2857–2863.
[55] A. Kashani, J.L. Provis, G.G. Qiao, J.S.J. van Deventer, The interrelationship between surface chemistry and rheology in alkali activated slag paste, Construct. Build. Mater. 65 (2014) 583–591.
[56] E.J. Teh, Y.K. Leong, Y. Liu, B.C. Ong, C.C. Berndt, S.B. Chen, Yield stress and zeta potential of washed and highly spherical oxide dispersions — critical zeta potential and Hamaker constant, Powder Technol. 198 (2010) 114–119.
[57] J. Nordström, A. Sundblom, G.V. Jensen, J.S. Pedersen, A. Palmqvist, A. Matic, Silica/alkali ratio dependence of the microscopic structure of sodium silicate solutions, J. Colloid Interface Sci. 397 (2013) 9–17.
[58] C.-X. Zhu, Recent Advances in Waterglass Sand Technologies, Research & Development, 2007, pp. 3–7.
[59] S.S.S.A. Nedunuri, S.G. Sertse, S. Muhammad, Microstructural study of Portland cement partially replaced with fly ash, ground granulated blast furnace slag and silica fume as determined by pozzolanic activity, Construct. Build. Mater. 238 (2020), 117561.
[60] Y.X. Pang, X.Q. Qiu, D.J. Yang, H.M. Lou, Influence of oxidation, hydroxymethylation and sulfomethylation on the physicochemical properties of calcium lignosulfonate, Colloids Surf. A Physicochem. Eng. Asp. 312 (2008) 154–159.
[61] M.M. Alonso, M. Palacios, F. Puertas, A.G. De La Torre, M.A.G. Aranda, Effect of polycarboxylate admixture structure on cement paste rheology, Mater. Construcción 57 (2007) 65–81.
[62] Y. Alrefaei, Y.-S. Wang, J.-G. Dai, The effectiveness of different superplasticizers in ambient cured one-part alkali activated pastes, Cement Concr. Compos. 97 (2019) 166–174.
[63] S. Tong, Z. Yuqi, W. Qiang, Recent advances in chemical admixtures for improving the workability of alkali-activated slag-based material systems, Construct. Build. Mater. 272 (2021), 121647.
[64] M. Palacios, F. Puertas, Stability of superplasticizer and shrinkage-reducing admixtures Stability of superplasticizer and shrinkage-reducing admixtures in high basic media, Mater. Construcción 54 (2004) 65–86.
[65] D. Feys, R. Verhoeven, G. De Schutter, Why is fresh self-compacting concrete shear thickening? Cement Concr. Res. 39 (2009) 510–523.
[66] B.J. Maranzano, N.J. Wagner, The effects of particle size on reversible shear thickening of concentrated colloidal dispersions, J. Chem. Phys. 114 (2001) 10514–10527.
[67] G. Bossis, J. Brady, The rheology of Brownian suspensions, J. Chem. Phys. 91 (1989) 1866–1874.
[68] M. Palacios, S. Gismera, M.M. Alonso, J.B. d'Espinose de Lacaillerie, B. Lothenbach, A. Favier, C. Brumaud, F. Puertas, Early reactivity of sodium silicate-activated slag pastes and its impact on rheological properties, Cement Concr. Res. 140 (2021) 106302.